Facet-specific Heterojunction in Gold-decorated Pyramidal Silicon for Electrochemical Hydrogen Peroxide Sensing

Chia-Wei Huang[1], Joey Andrew A. Valinton[2], Yung-Jr Hung[1] and Chun-Hu Chen*[2]
Department of Photonics, National Sun Yat-sen University, Kaohsiung, Taiwan 80424.
Department of Chemistry, National Sun Yat-sen University, Kaohsiung, Taiwan 80424.
E-mail: chunhu.chen@mail.nsysu.edu.tw; Tel: +886-7-525-2000

A B S T R A C T

Nanoscale heterojunction of asymmetrical band structures and electron distributions at the interfaces is critical for activity enhancement in various catalytic applications. However, realization of facet-specific heterojunction remains challenging; yet it has been rarely studied in electrocatalysis. In this work, we first report the enhanced electrocatalytic performance of monolith Au/Si (111) heterojunction on Si micron-scale pyramids, prepared by alkaline Si-wafer etching with surface decoration of isolated gold nanoparticles (5-15 nm). The Au/Si (111) heterojunction exhibits the facet-dependent electrochemical activities superior to Au/Si (100). Varied Si etching levels enable the mixed exposure of Si (111) and Si (100); and the results further support the facet-dependent electrochemical enhancement. By excluding the effects of surface areas and defects, studies on the role of Si (111) reveal that the Au/Si (111) interface is very essential in improving the sensitivity and the detection limit at the heterojunction. This means that usage of well-controlled facets instead of merely facilitating electron transport can be considered in heterojunction electrocatalyst design. The H_2O_2 sensing performance of Au/Si (111) is synergistically enhanced achieving 194 times greater sensitivity than the Au/Si (100) with a wide linear range from 0.01 to 55.55 mM, high sensitivity (171 $\mu A\ mM^{-1}\ cm^{-2}$), and low detection limit of 1.24 µM.

Key words: Pyramidal silicon, gold, hydrogen peroxide, electrochemical, Si (111), heterojunction.

1. Introduction

Heterojunctions of diverse materials feature asymmetrical combinations of band structures, lattice strain, and elemental distributions at the interfaces to enhance the different properties of materials. Heterojunction design for increasing catalytic activity includes decorating nanocatalysts on frameworks that can improve the electron transfer to and from the catalyst [1-3]. Apparently, various catalytically-active facets and facile routes towards single-faceted surfaces have been realized [4-6]; thus, heterojunction design can be employed to such materials in which it provided a synergistic effect at the interfaces producing better catalytic properties [7, 8]. Well controlled heterojunctions have been demonstrated for enhancing photo- [7, 9] and electrocatalytic [10-14] performance with the interfaces where at least one contains a single-faceted crystalline surface. Synthesis of such heterojunction electrocatalysts includes complicated methods such as molecular beam epitaxy [11, 12] and ultrahigh vacuum deposition [15]. Galvanic displacement [13, 16] employs easier deposition of materials on surface with a uniform facet, but poses risks on maintaining facet integrity due to corrosion of the surface in the premise that the metal to be deposited, typically noble metals, would displace the oxidized region. Therefore, a more facile route towards formation of heterojunctions while maintaining the integrity of the facet is highly desired.

Silicon is an earth-abundant material with attractive properties of beneficial surface tailorability, biocompatibility, and extraordinary electrical/mechanical performance [17-19]. Si (100) wafers have been commercialized worldwide as standard substrates for the semiconductor industry. Emerging techniques are desired to develop based on Si wafers for potential commercialization. Different types of texturing pathways on Si wafers have been developed, such as metal-assisted chemical etching (MACE), alkaline etching, and many others [20-22]. These approaches utilize anisotropic etching rates between crystal planes of Si wafers to generate diverse features. In Si-based solar cells and devices, anti-reflective layers comprised of pyramidal Si textures via alkaline etching are widely introduced in both academia and industry to increase power conversion efficiency [21]. These works concentrate on

the establishment of rough Si surface with low defects, yet the monolith facet orientation of Si (111) has not been recognized. Recent work by Man and coworkers reported the gold and silver full coating on Si pyramids for surface enhanced Raman study [22]. The focus of the study concentrated on the roughness investigation of Si pyramids, rather than utilization of the buried Si (111). In fact, beyond the anti-reflection and surface roughness, Si pyramidal textures are excellent candidates to achieve scalable facet-specific substrate without the presence of impure crystal planes. However, a few studies involving etched Si heterojunctions at which a uniform Si facet is fabricated to explore facet-dependent catalytic and sensing capabilities [23, 24].

Hydrogen peroxide (H_2O_2) is a metabolic byproduct that serves as a key regulator for a number of oxidative stress-related states and certain intracellular pathways [25]. In addition, precise determination of hydrogen peroxide is important in the areas of environmental protection [26, 27], food safety [28], and pharmaceutical industry [29]. Hydrogen peroxide sensing techniques, such as titrimetry [30], spectrophotometry [31], chemiluminescence [26], fluorescence [27], and electrochemical methods have been reported. Electrochemical sensors based on noble metals [32-34] and transition metal oxides [35-37] exhibit promising activities toward H_2O_2 detection due to the advantages of rapid response and simple operation. In terms of electrocatalyst design, surface area enlargement becomes the major concern to improve the electrocatalytic performance. Zhong et al. demonstrated the improved sensing activities by Ag/Si nanowire heterojunction with high specific surface area [38]. Similar concepts based on high surface-area nanostructures were reported with examples of Au/Pt/C nanotubes [2], Pt/TiO_2/C nanotubes [1], and $Ni(OH)_2$/Si nanowires [39], although facet-dependent electrocatalysis was not acknowledged among these studies. Despite the well recognition of facet-specific heterojunction in many catalytic fields, [14, 40] systematic study of the heterojunction concept in electrocatalysis is rare. The inter-correlated effects of surface areas and random-facet heterojunction further hinder the understanding of facet-specific heterojunction electrocatalysis.

In this work, we first report the scalable fabrication of gold-decorated pyramidal Si (111) heterojunction exhibiting a higher sensitivity and lower detection limits as compared to other Si-based heterojunctions. The monolith Au/Si (111) exhibits the facet-dependent electrochemical performance superior to Au/Si (100), emphasizing the importance of facet-specific heterojunction to realize high-performance sensor design. The experimental approaches such as comparison of exposed surface area, incremental blockage of heterojunction interface, and determination of facet defects verify the enhancement contribution of the heterojunction interfaces. This study would gain interest towards design of well-controlled heterojunctions in electrocatalysis.

2. Experiment

2.1. Reagents

The chemicals of dopamine (DA), ascorbic acid (AA), and uric acid (UA) were obtained from Alfa Aesar. Hydrogen peroxide solution (30%) was purchased from Katayama Chemical Industry company. Sodium dihydrogen phosphate (NaH_2PO_4) and disodium hydrogen phosphate (Na_2HPO_4) were purchased from Panreac Co. The highly-doped Si (100) wafers were purchased from Summit-Tech Co.

2.2. Fabrication of Au-decorated pyramidal Si electrodes

First, the highly-doped p-type single crystal silicon (100) wafer (0.001 − 0.005 Ω cm) was cleaned by ultrasonication in acetone, isopropanol (IPA), and deionized (DI) water consecutively. Before alkaline etching, the silicon wafers were immersed in a HF solution for 30 seconds at room temperature to remove native-oxide layer, then rinsed by DI water thoroughly, and dried by N_2. The as-cleaned Si (100) wafers were textured by aqueous etching under the mixtures of tetramethylammonium hydroxide (TMAH, 25%): IPA: DI water of 23:20:120 ml at 85^{o}C with agitation for 15 min (under etched), 25 min (ideal etched), 35 min (over etched). The samples were

rinsed by DI water and dried by N_2 after the etching step. To clean out any potential organic residues, UV Ozone cleaner (SAMCO, UV−1) was used to treat samples for 30 minutes at 100°C. The cleaned wafers were immersed in a HF solution for 30 seconds at room temperature to remove surface oxide layer and promote Au adhesion. The etched wafers were then placed in an electron beam evaporator for gold nanoparticle deposition under a pressure of 2×10^{-6} torr, yielding the gold-decorated pyramidal Si electrodes (GPS). The deposition rate for GPS is 0.2 Å/sec for 250 seconds. Control samples were also fabricated with longer gold deposition on pyramidal Si for for 500 seconds (GPS_{2x}), 1000 seconds (GPS_{4x}), and 1500 seconds (GPS_{6x}), representing the original deposition time multiplied by two, four, and six, respectively.

2.3. Characterization and electrochemical measurement

The surface morphology of the gold and pyramidal Si was monitored by a FEI Inspect™ F50 Schottky field emission scanning electron microscope (FE-SEM) with an acceleration voltage of 5 kV. Raman spectra were acquired using a WITec Confocal Raman Microscope Alpha300R with a 532 nm laser.

For the electrochemical measurements, a CHI 614D electrochemical analyzer was used with a conventional three-electrode configuration of Ag/AgCl (saturated NaCl) as the reference electrode and Pt plate as the counter electrode. The total surface area of all the prepared electrodes used in this study was 1×1 cm^2. In a typical hydrogen peroxide sensing experiment, amperometic measurements were carried out under various concentrations of H_2O_2 solution (ranging from 0.01 mM to 5 mM) that were injected into a 0.1 M phosphate buffer solution (PBS) at pH =7.2. One minute was given to each injection to achieve an equilibrated response. Interference studies were also conducted where 100 µL samples of 1 mM dopamine, 1 mM uric acid, 1 mM ascorbic acid, 5 mM glucose and 1 mM acetaminophen were spiked over the solution comparing with 6.9 µL H_2O_2 upon measuring the i-t curve.

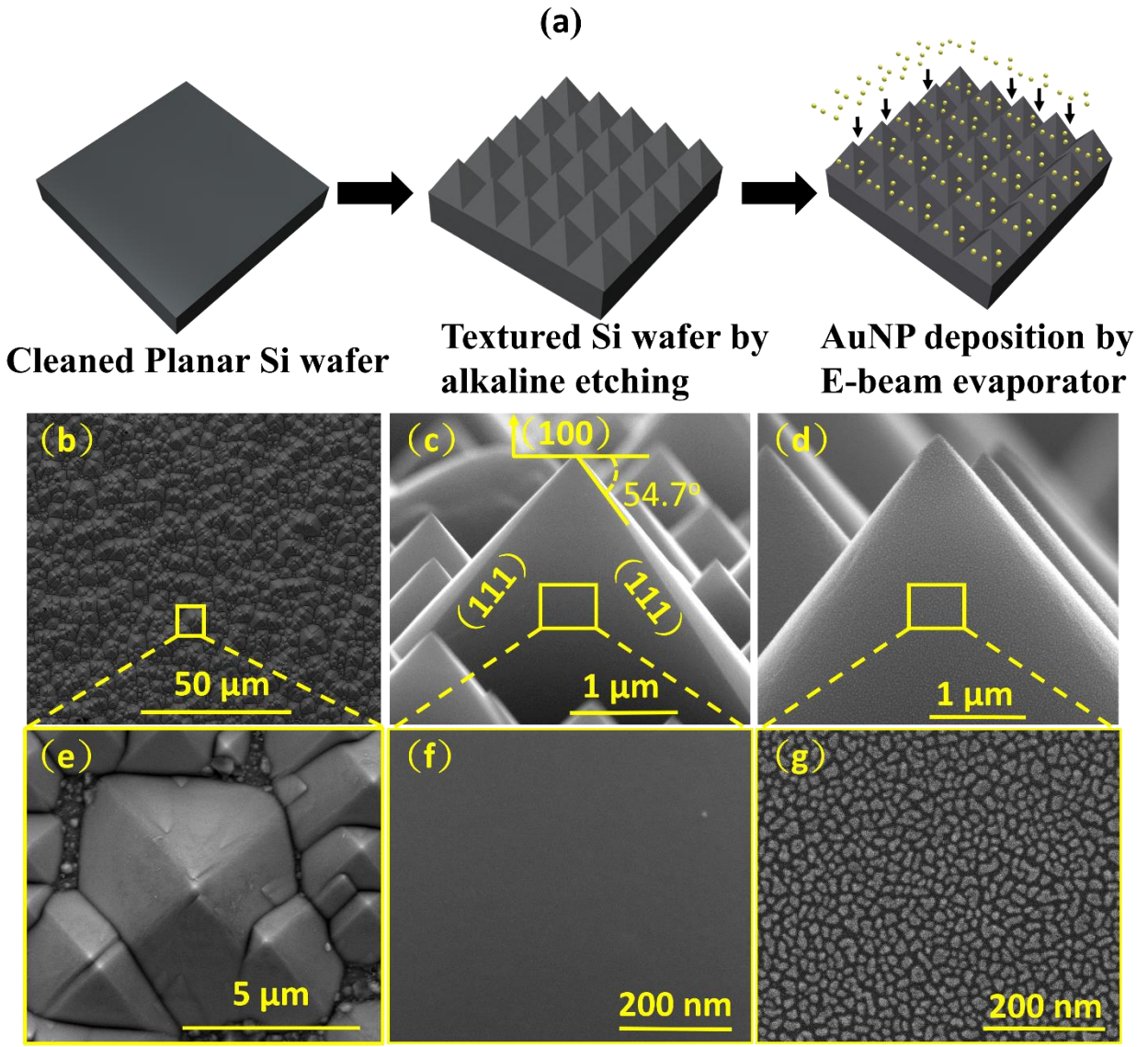

Fig. 1. Schematic illustration of fabrication procedures of gold-decorated pyramidal Si (GPS) wafer (a), and the SEM images of GPS samples. (b-g). (b) The top view of pyramidal structures of Si over a hundred micron; (c) The cross-section view of the Si pyramids; (d) The cross section view of GPS. The images of in (e), (f), (g) are the enlarged images corresponding to the yellow rectangles in (b), (c), (d), respectively.

.

3. Results

The fabrication process of GPS is illustrated in Fig. 1a. The anisotropic etching on a pristine Si (100) wafer results in the square-like pyramidal arrays. Fig. 1b shows the SEM images of top views

of ideal pyramidal Si arrays over an area of 100 × 100 μm^2 after the alkaline etching. The zoomed-in images (Fig. 1e) clearly demonstrate the formation of individual Si pyramid with different sizes, suggesting a kinetic-dependent etching process. We conducted the cross-sectional observation of the individual Si pyramid shown in Fig. 1c. Since Si conforms to a simple cubic lattice, the interplanar angles can be measured using the following equation [41]:

$$\cos\phi = \frac{h_1h_2+k_1k_2+l_1l_2}{\sqrt{(h_1^2+k_1^2+l_1^2)(h_2^2+k_2^2+l_2^2)}} \quad (1)$$

where Miller indices are referred to as (h_1 k_1 l_1) and (h_2 k_2 l_2), and the theoretical interplanar angle between (111) and (100) is calculated to be 54.7º. Upon measuring the angle between the slope of the pyramid and the tangent line on the apex of the Si pyramid, an interplanar angle of 54.7º was measured. Since the plane tangent to the apex is the Si (100) plane corresponding to the starting material, these results verify the presence of Si (111) on the edges of Si pyramids [42]. The images of Si (111) show the smooth surface without appreciable residue contamination or defects (Fig. 1f). After the Au deposition on Si pyramids, the pyramidal shapes remain identical (Fig. 1d) while the Si (111) surface is homogeneously decorated with the isolated gold nanoparticles with diameters of 5-15 nm (Fig. 1g). These gold-decorated pyramidal Si (GPS) electrodes successfully create the Au/Si (111) nanoscale heterojunction accessible for electrocatalysis.

3.1. Electrocatalysis of Au/Si (111) heterojunction

The electrocatalytic performances of GPS electrodes for H_2O_2 reduction were first evaluated by cyclic voltammetry [43]. The utilization of reduction signals, rather than oxidation ones, was adopted to avoid the potential sensing interference [44]. To understand the pyramidal structure effect, the cyclic voltammograms (CVs) of the planar Si (pristine Si (100) wafer surface without any etching) and pyramidal Si electrodes in the absence and presence of 5 mM H_2O_2 were shown in Fig. 2a. The increases of reduction currents can be clearly observed with the presence of H_2O_2. The greater current

increase of pyramidal Si electrodes, 2.5 to 3 times higher than planar Si, indicates the stronger electroreduction activities. In addition, the lowered onset potentials at -0.04 V in GPS (vs. about -0.2 V for planar Si) demonstrate a relatively low energy barrier required to initiate H_2O_2 reduction. All the data show the higher electrocatalytic activities of Si (111) pyramids than Si (100). To further compare their performances after the identical gold-decoration, Fig. 2b shows the CVs of planar Au/Si (100) and pyramidal Au/Si (111) in the absence and presence of 5 mM H_2O_2. Au/Si (111) shows a greater amperometric increase (around 600 μA) at -0.5 V, while that of Au/Si (100) is negligible. The drastic current enlargement after gold decoration on Si (111) indicates that Au/Si (111) heterojunction creates the active sites responsible for the electrocatalytic enhancement. Therefore, the superior electrocatalytic performance of Au/Si (111) was selected for the further H_2O_2 sensing studies.

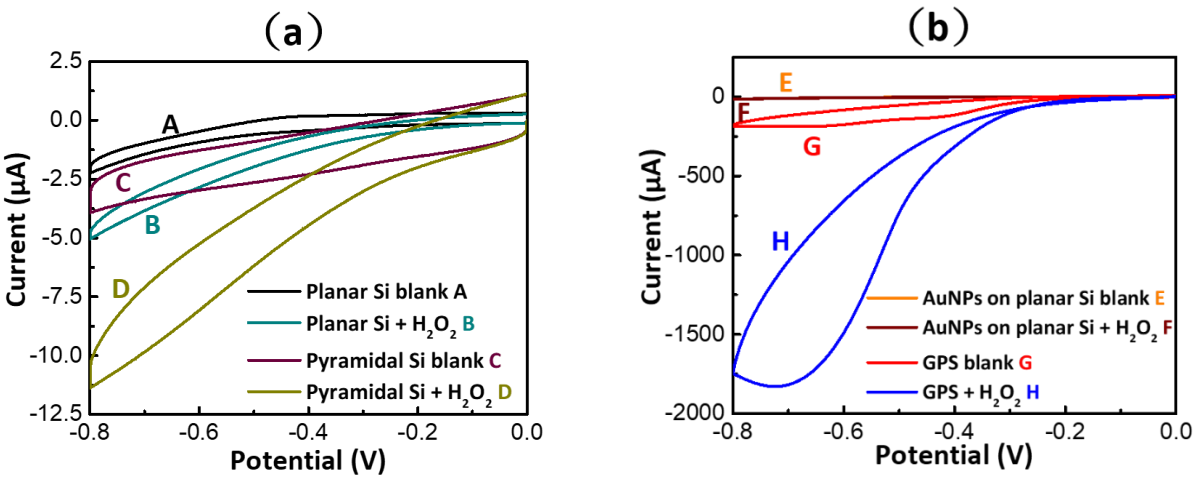

Fig. 2. The cyclic voltammograms (CVs) comparison of planar and pyramidal Si electrodes in the absence (the "blank" denotation of A, C, E, and G curves) and presence of 5 mM H_2O_2 (B, D, F, and H curves) in 0.1 M PBS (pH=7.2) with a scan rate of 50 mVs^{-1}. (a) The planar (pristine) Si (100) and pyramidal (alkaline-etched) Si (111) electrodes; (b) the Au-decorated planar Si (100) and GPS electrodes.

3.2. H_2O_2 sensing

We investigated the optimal applied potentials of GPS electrodes by measuring current responses under 0.1 M PBS (pH=7.2) with the successive addition of the H_2O_2. Fig. 3a presents the

amperometric responses (i-t curves) of GPS at applied potentials of -0.4 V, -0.5 V, and -0.6 V with the corresponding calibration curves as shown in Fig. 3b. The stepwise amperometric changes exhibit the sensing capability of GPS electrodes in which the results were shown in Table 1. According to Table 1, the sensitivity of GPS at -0.4 V is smaller compared to those at -0.5 V and -0.6 V which clearly makes it not a suitable potential to be used for optimal sensing performance. The measurements at -0.6 V show noisier signals and more rapid saturation compared to those at -0.5 V.

Moreover, amperometric (i-t) curves have also been measured at -0.45 V and -0.55 V (Fig. S1) to further determine the optimum applied potential to be used. Calibration curves for the two potentials were compared with -0.5 V (Fig. S2) whose values were summarized in Table S1. The sensitivity at -0.55 V is comparable with -0.5 V, yet it suffers the same saturation and signal problems as -0.6 V. Meanwhile, the sensitivity of -0.45 V is still low despite its closeness to the sensitivity at -0.5 V. Therefore, the highest sensitivity and smallest detection limits can be achieved at -0.5 V making it as the optimal applied potential chosen for sensor operation.

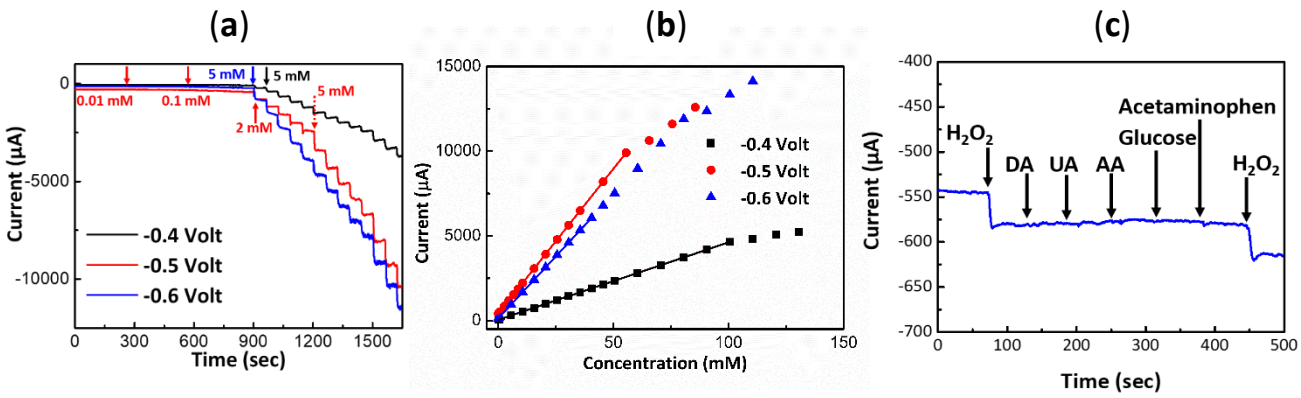

Fig. 3. (a) The amperometric response (i-t curve) of the GPS electrode, **(b)** The calibration curves corresponding to the data of (a) upon successive addition of H_2O_2 at various potentials of -0.4 V to -0.6 V in 0.1 M PBS (pH = 7.2). **(c)** The i-t curves for the interference studies of GPS with the presence of interfering species of 0.1 mM DA, UA, AA, acetaminophen, and 5 mM glucose at -0.5 V.

Table 1. Comparison of the performance at different applied potentials −0.4 V, −0.5 V, and −0.6 V.

Potential (V)	Sensitivity (μA/mM cm^{-2})	Detection limit (μM)	Linear range (mM)
-0.4	44.6	2.02	0.01 – 100.55
-0.5	171	1.24	0.01 – 55.55
-0.6	146	1.31	0.01 – 40.55

Interference studies on GPS were carried out to determine the selectivity of GPS towards hydrogen peroxide. Possible interferences may be caused by common chemical species which includes ascorbic acid (AA), uric acid (UA), dopamine (DA), glucose, and acetaminophen [43, 44]. As shown in Fig. 3c, the amperometric response brought by the addition of the possible interferences produce a negligible change in current as compared to the huge change upon the addition of H_2O_2, showing the excellent selectivity of GPS toward detecting H_2O_2.

4. Discussion

4.1. Facet-dependent activities of pyramids

The precise controls of ideal pyramidal microstructures are strongly related to chemical etching process and reagent diffusion kinetics which can influence the degrees of anisotropy and size distribution of Si pyramidals [45] Varied sizes of Si pyramids may be obtained yet the selective exposure of Si (111) can be effectively achieved. [46] We studied the correlation between electrochemical activities and Si texture evolution. By reducing the etching time from 25 to 15 minutes, the under-etched samples show the lowered pyramid densities with shorter pyramid heights (Fig. 4a). On the other hand, over-etching Si for 35 minutes flattened the sharp tips of pyramids which eventually exposed the Si (100) facet parallel to the pristine wafer surface with the visible facet contamination on Si (111) edge (see Fig. 4b). Consequently, the CV of the under-etched (Fig. 4c) and over-etched (Fig. 4d) samples both result in the weaker electrochemical responses in the presence of H_2O_2. In addition, the H_2O_2 sensing calibration curves of pyramidal Si (111) and planar Si (100), as shown in Fig. 5a, derived from the amperometric (i-t) curves (Fig. S3) suggests that Si (111) has 6.8 times higher

sensitivity than Si (100). Based on the pyramid dimensions in SEM images, the surface area of Si (111) pyramids is estimated via geometry to be no greater than twice of planar Si (100). Moreover, the morphologies of the deposited gold on Au/Si (100) are similar compared to Au/Si (111) which means that the coating of Au in each of the Au/Si catalysts are even regardless of the facet differences (Fig S5). With the activity enhancement much greater than the increase of surface area from Si (100) to Si (111), this indicates that surface area is not the governing effect on the sensitivity improvement.

Another concern is regarding the consequences of etching, specifically the presence of dangling bonds (i.e., Si-H species) and/or surface crystal defects which could potentially act as active sites to enhance the surface reactivity [47]. We used Raman spectroscopy to monitor surface defects by comparing linewidth and intensity of Si-Si bonds (at 520 cm^{-1}) and dangling bonds of Si-H species (at 630 cm^{-1} and 2000 cm^{-1}) [48, 49]. Fig. 6 shows the Raman spectra of Si (100) and Si (111) pyramids, which are nearly superimposed to each other. The zoom-in spectra (corresponding to Si-H species) in Fig. 6b and Fig. 6c further verify their negligible difference. Furthermore, the density of dangling bonds on the Si (100) and Si (111) was reported to be roughly the same (1.5×10^{15} cm^{-2}) with the normalization of surface areas [50, 51]. These results suggest that the activity difference between pyramidal Si (111) and planar Si (100) is mainly attributed to the exposed facets, rather than the effects of surface areas or defects. These properties between the facets might be associated with the literature that Si (111) exhibited the greater electron mobility than Si (100) [52, 53], leading to the facet-dependent electrocatalysis as observed.

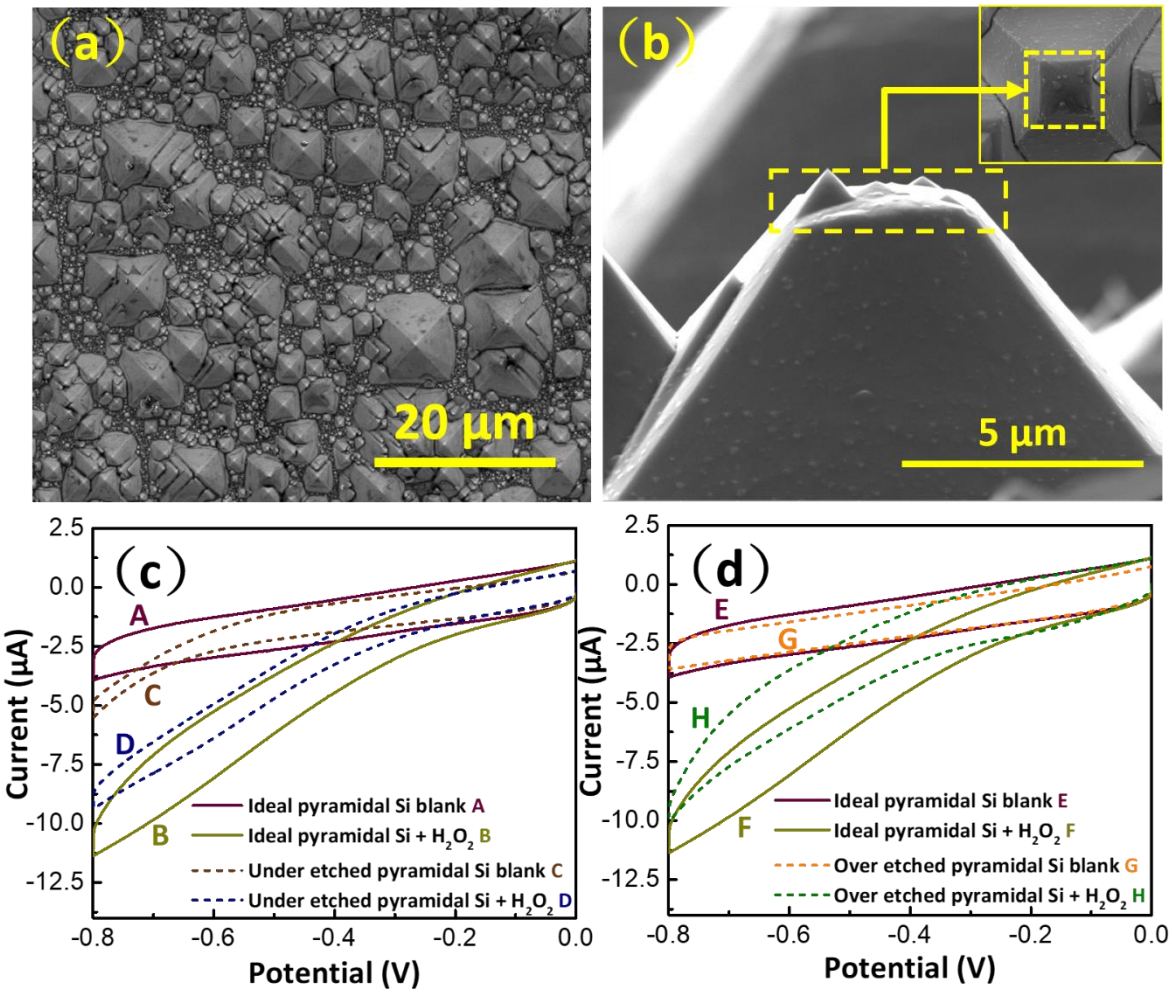

Fig. 4. SEM images of (a) the under-etched (15 min) and (b) the over-etched pyramidal Si (35 min). The inset in (b) is the top view of the over-etched pyramids. The cyclic voltammograms (CVs) of under-etched (c) and over-etched (d) Si electrodes in comparison with ideal pyramidal Si (111). The tests were conducted in the absence (the "blank" denotation of A, C, E, and G curves) and presence of 5 mM H_2O_2 (B, D, F, and H curves) in 0.1M PBS (pH=7.2) with a scan rate of 50 mVs^{-1}.

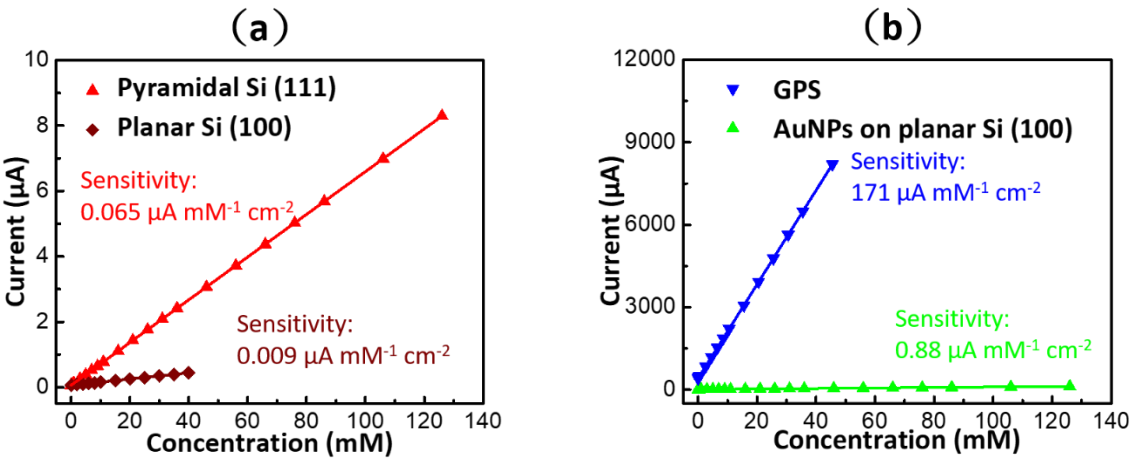

Fig. 5. (a) The corresponding calibration curves of pristine Si (100) (brown line) and pyramidal Si (111) (red line); (b) the corresponding calibration curves of GPS (Au/Si (111)) electrode (blue line) and AuNPs on pristine Si (Au/Si (100)) electrode (green line).

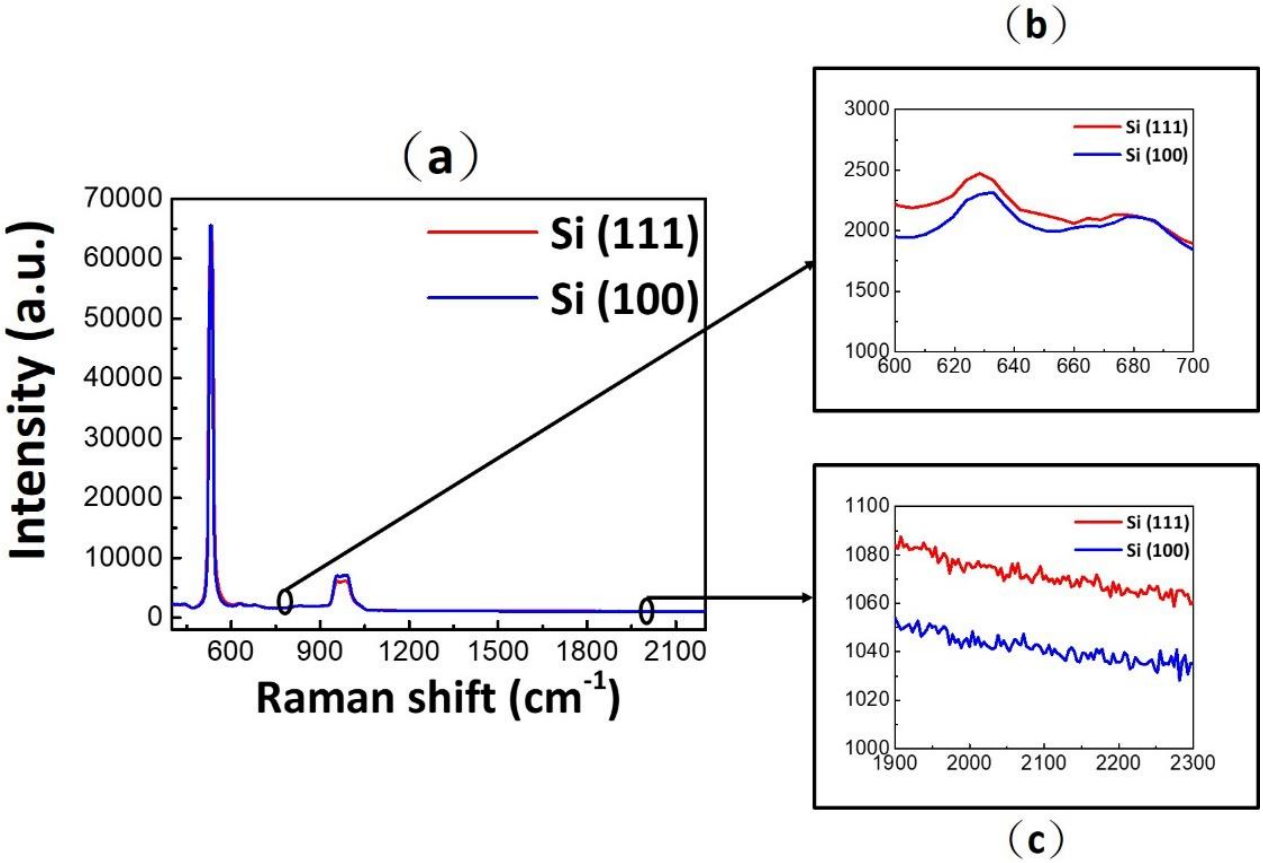

Fig. 6. The Raman spectra of Si (100) and Si (111) (a). The zoom-in comparison of Si-H bonds at 630 cm^{-1} (b) and 2000 cm^{-1} (c).

4.2. Enhancement effect at heterojunctions

The comparison of Au-decorated planar Si (100) (green line) and GPS (blue line) is shown in Fig. 5b, based on the amperometric (i-t) curves in Fig. S4. It shows that the sensitivity of GPS can be about 194 times greater than the Au/Si (100). This huge difference in sensitivity exceeds drastically in comparison with the difference between bare Si (100) and Si (111) without gold decoration, suggesting that the heterojunction sites between the deposited Au and different Si facets play the key role in obtaining the high electrocatalytic performance. To prove such point, we have conducted experiments to vary the Au/Si (111) interfacial sites by increasing the time for Au deposition. Different electrodes whose deposition times were increase by two-fold (GPS_{2x}), four-fold (GPS_{4x}) and six-fold (GPS_{6x}) to GPS were prepared. As shown by the SEM images in Fig. 7a-f, the gradual decline of the exposed heterojunction can be observed with the increase of the Au deposition time. The close-up images of the surface in GPS_{4x} and GPS_{6x} clearly shows the absence of low contrast regions which pertains to the surface of Si pyramidals. Consequently, usage of these samples for amperometric H_2O_2 sensing (Fig. 7g-i) indicates the decrease in the sensitivities and an increase in the detection limits (Table 2) with the prolonged deposition time.

GPS, in terms of electrochemical H_2O_2 sensing, have provided the highest sensitivity and the lowest detection limit among its other electrode variants. This suggests that the exposed Au/Si (111) interfaces serve as the active sites for electrocatalysis. The metal-semiconductor interface like Au/Si(111) creates a Schottky junction in which there is a distortion in the band structure causing unique catalytic properties [54]. In addition, the p-type nature of Si (111) influences the Au layer which could possibly increase the charge separation between Au and Si (111). This separation of charge also happened to n-type Si (111) and Pt where the Schottky junction facilitated the oxidation of $Ni(OH)_2$ to NiOOH in the interface together with a relatively high sensitivity towards H_2O_2 photoelectrochemical sensing [23]. Due to the absence of any surface deformities on Si (111) together with the Au/Si (111) deposition studies, it may suggest that the catalytically active site happens at the

interface due to the charge separation and the band bending between the two materials. This kind of interaction has long before exhibited when the Au (111) and Si (111) interface produced a much better electron transmissivity than its Au (111)/Si (100) homologue based on ballistic electron transport studies [52]. In addition, the electron mobility through the Au/Si interface was observed to decrease as the thickness of the Au increases because the Schottky barrier created between Au/Si results into scattering of electrons as it passes through it. This electron mobility phenomena has also been exhibited to a similar study between the interaction of different facets of Si in conjunction with a Pd film [55]. The improvement of electron mobility at the interface obtains an increase of the reduction current generated which improves the sensitivity of the GPS electrode towards H_2O_2. Increasing the Au deposition which results in a bulky layer with the diminished exposure of heterojunction interface leads to poorer sensitivity. In comparison with some reported Si-nanowire based H_2O_2 electrochemical sensors (Table 3) where no facet-selective heterojunction with Ag/Au nanoparticles and Ni oxides was fabricated, GPS exhibits the higher or comparable sensing performance although it suffers from the much smaller surface areas than that of the Si nanowire sensors. Therefore, usage of well-controlled facets in design of heterojunctions should be emphasized to improve electrochemical performance. The synergistic effect of the heterojunction interface is recognized to be critical in electrochemical catalysis.

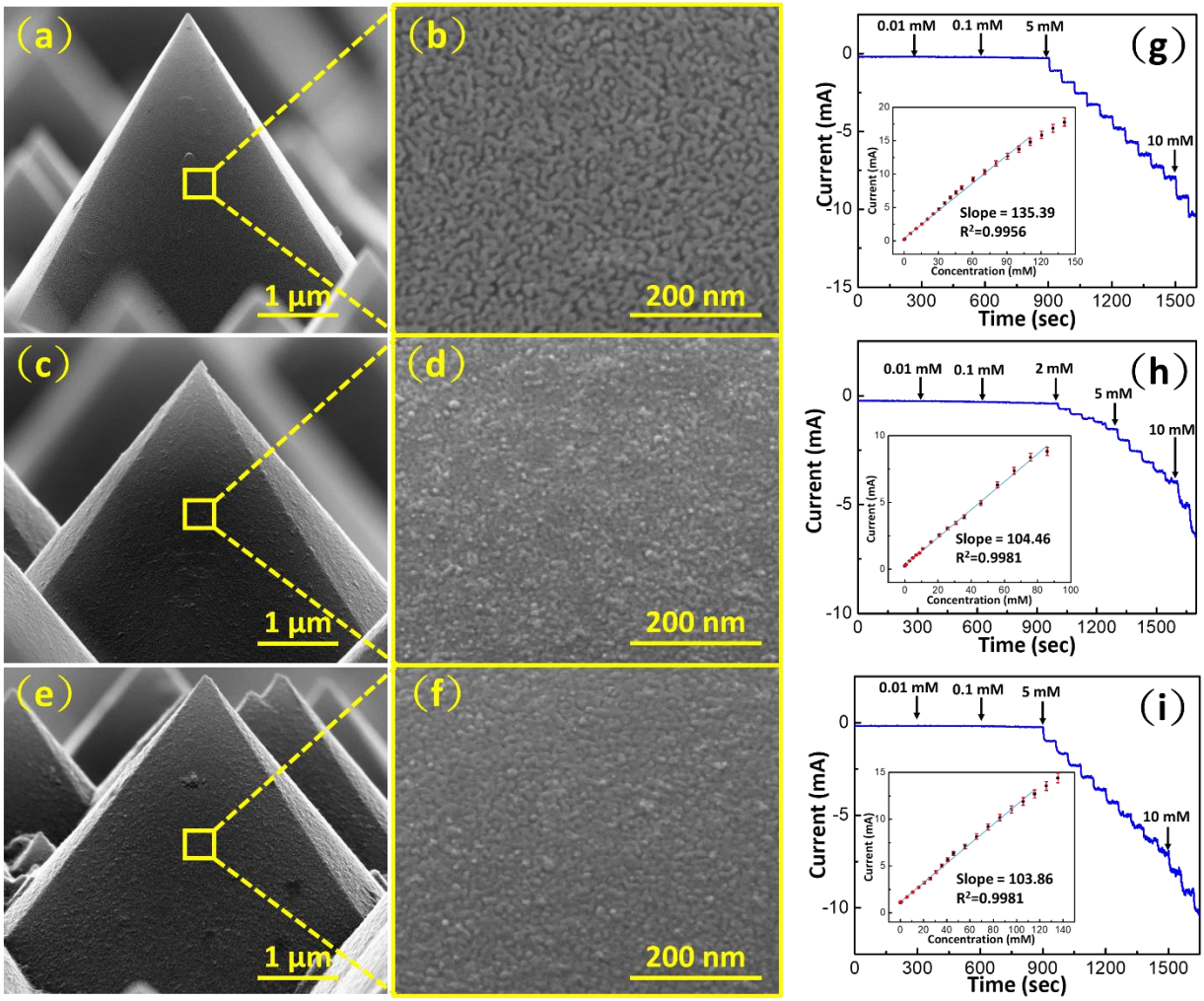

Fig. 7. The SEM images of GPS_{2x}, GPS_{4x}, and GPS_{6x}. (a-f). The cross-section view of (a) GPS_{2x}, (c) GPS_{4x}, and (e) GPS_{6x}; The images of in (b), (d), (f) are the enlarged images corresponding to the yellow rectangles in (a), (c), (e), respectively. (g), (h), and (i) are amperometric responses of GPS_{2x}, GPS_{4x}, and GPS_{6x} upon successive addition of H_2O_2 at applied potential -0.5 V, respectively. The insert images of in (g), (h), and (i) are the corresponding calibration curves of GPS_{2x}, GPS_{4x}, and GPS_{6x}, respectively.

Table 2. Comparison of the performance of GPS, GPS_{2x}, GPS_{4x}, and GPS_{6x}.

Sample	Sensitivity (μA/mM cm^{-2})	Detection limit (μM)	Linear range (mM)
GPS	171	1.24	0.01 – 55.55
GPS_{2x}	135	2.05	0.01 – 110.55
GPS_{4x}	104	3.35	0.01 – 85.80
GPS_{6x}	104	4.30	0.01 – 115.55

Table 3. Comparison of the performance of various H_2O_2 sensors. *photoelectrochemical sensor

Electrode	Detection limit	Sensitivity	Linear range	Reference
AuNPs@SiNWs	—	—	20 – 1000 μM	[56]
AgNPs/p-SiNWs	0.2 μM	8.96 μA mM^{-1} cm^{-2} / 57.5 μA mM^{-1} cm^{-2}	0.2 – 70 mM / 0.2 – 20 mM	[38]
Ag nanodendrites/SiNWs	—	35.88 μA mM^{-1} cm^{-2}	0.05 – 16.5 mM	[57]
$Ni(OH)_2$/SiNWs	3.2 μM	3.31 mA mM^{-1} cm^{-2}	0 – 55 mM	[39]
NiOOH/Pt/n-n+-Si*	2.2 μM	229 μA mM^{-1} cm^{-2}	0.01–0.06 mM	[23]
GPS	1.24 μM	171 μA mM^{-1} cm^{-2}	0.01 – 55.55 mM	This work

5. Conclusion

Through the controlled alkaline etching processes of Si wafers, the facet-dependent heterojunction of Au/ Si (111) pyramids have been successfully fabricated exhibiting the H_2O_2 sensitivity by 194 times greater than Au/Si (100). With the eliminated influence of surface areas and defects, the studies of under- and over-etched Si pyramids verify the facet-dependent electrocatalysis between Si (111) and Si (100). After the formation of Au/Si (111) heterojunction, the synergistic electrochemical performance can be observed in GPS. By gradually blocking all the accessible heterojunction sites with continuous gold coating, the inhibited sensing performance further confirms that the Au/Si (111) interface mainly contributes to the electrocatalytic enhancement. Our results emphasize the importance

of facet-specific heterojunction fabrication in the future designs of electrochemical sensors. Apart from the conventional concepts of gaining high surface areas and conductivity in electrocatalysts, the usage of facet-controlled interfaces for high performance electrocatalysis should also be considered. Moreover, our approach demonstrated a simple, reliable protocol of utilizing commercial Si wafers to study facet-dependence in various electrocatalysis.

Acknowledgement

We thank the funding support from Ministry of Science and Technology, Taiwan under Grant No. MOST 105-2113-M-110-003 and MOST 105-2221-E-110-075.

References

[1] X. Pang, D. He, S. Luo, Q. Cai, An Amperometric Glucose Biosensor Fabricated with Pt Nanoparticle-Decorated Carbon Nanotubes/TiO2 Nanotube Arrays Composite, Sens. Actuators, B, 137 (2009) 134-138.

[2] X. Niu, H. Zhao, C. Chen, M. Lan, Platinum Nanoparticle-Decorated Carbon Nanotube Clusters on Screen-Printed Gold Nanofilm Electrode for Enhanced Electrocatalytic Reduction of Hydrogen Peroxide, Electrochim. Acta, 65 (2012) 97-103.

[3] Y. Sun, K. He, Z. Zhang, A. Zhou, H. Duan, Real-Time Electrochemical Detection of Hydrogen Peroxide Secretion in Live Cells by Pt Nanoparticles Decorated Graphene–Carbon Nanotube Hybrid Paper Electrode, Biosens. Bioelectron., 68 (2015) 358-364.

[4] D.W. Hatchett, H.S. White, Electrochemistry of Sulfur Adlayers on the Low-Index Faces of Silver, J. Phys. Chem., 100 (1996) 9854-9859.

[5] E. Sitta., A.M. Gómez-Marín, A. Aldaz, J.M. Feliu, Electrocatalysis of H_2O_2 Reduction/Oxidation at Model Platinum Surfaces, Electrochem. Commun., 33 (2013) 39-42.

[6] M.M. Najafpour, S.M. Hosseini, Z. Zand, Manganese Oxide Supported on Gold/Iron as a Water-Oxidizing Catalyst in Artificial Photosynthetic Systems, Dalton Trans., 45 (2016) 9201-9208.

[7] X.-j. Wang, W.-y. Yang, F.-t. Li, J. Zhao, R.-h. Liu, S.-j. Liu, B. Li, Construction of Amorphous TiO2/BiOBr Heterojunctions via Facets Coupling for Enhanced Photocatalytic Activity, J. Hazard. Mater., 292 (2015) 126-136.

[8] R. Li, H. Han, F. Zhang, D. Wang, C. Li, Highly Efficient Photocatalysts Constructed by Rational Assembly of Dual-Cocatalysts Separately on Different Facets of BiVO4, Energy Environ. Sci., 7 (2014) 1369-1376.

[9] L. Sun, L. Xiang, X. Zhao, C.-J. Jia, J. Yang, Z. Jin, X. Cheng, W. Fan, Enhanced Visible-Light Photocatalytic Activity of BiOI/BiOCl Heterojunctions: Key Role of Crystal Facet Combination, ACS Catal., 5 (2015) 3540-3551.

[10] I.E.L. Stephens, A.S. Bondarenko, F.J. Perez-Alonso, F. Calle-Vallejo, L. Bech, T.P. Johansson, A.K. Jepsen, R. Frydendal, B.P. Knudsen, J. Rossmeisl, I. Chorkendorff, Tuning the Activity

of Pt(111) for Oxygen Electroreduction by Subsurface Alloying, J. Am. Chem. Soc., 133 (2011) 5485-5491.

[11] T. Wadayama, N. Todoroki, Y. Yamada, T. Sugawara, K. Miyamoto, Y. Iijama, Oxygen Reduction Reaction Activities of Ni/Pt (111) Model Catalysts Fabricated by Molecular Beam Epitaxy, Electrochem. Commun., 12 (2010) 1112-1115.

[12] F. Besenbacher, I. Chorkendorff, B.S. Clausen, B. Hammer, A.M. Molenbroek, J.K. Nørskov, I. Stensgaard, Design of a Surface Alloy Catalyst for Steam Reforming, Science, 279 (1998) 1913-1915.

[13] J. Zhang, M.B. Vukmirovic, Y. Xu, M. Mavrikakis, R.R. Adzic, Controlling the Catalytic Activity of Platinum-Monolayer Electrocatalysts for Oxygen Reduction with Different Substrates, Angew. Chem. Int. Ed., 44 (2005) 2132-2135.

[14] B. Wu, N. Zheng, Surface and Interface Control of Noble Metal Nanocrystals for Catalytic and Electrocatalytic Applications, Nano Today, 8 (2013) 168-197.

[15] Q. Fu, W.-X. Li, Y. Yao, H. Liu, H.-Y. Su, D. Ma, X.-K. Gu, L. Chen, Z. Wang, H. Zhang, B. Wang, X. Bao, Interface-Confined Ferrous Centers for Catalytic Oxidation, Science, 328 (2010) 1141-1144.

[16] S.M. Alia, Y.S. Yan, B.S. Pivovar, Galvanic Displacement as a Route to Highly Active and Durable Extended Surface Electrocatalysts, Catal. Sci. Technol., 4 (2014) 3589-3600.

[17] Y. Cui, Q. Wei, H. Park, C.M. Lieber, Nanowire Nanosensors for Highly Sensitive and Selective Detection of Biological and Chemical Species, Science, 293 (2001) 1289-1292.

[18] Y. Cui, C.M. Lieber, Functional Nanoscale Electronic Devices Assembled Using Silicon Nanowire Building Blocks, Science, 291 (2001) 851-853.

[19] J. Liu, Q. Zhang, T. Zhang, J.-T. Li, L. Huang, S.-G. Sun, A Robust Ion-Conductive Biopolymer as a Binder for Si Anodes of Lithium-Ion Batteries, Adv. Func. Mater., 25 (2015) 3599-3605.

[20] Z. Huang, N. Geyer, P. Werner, J. de Boor, U. Gösele, Metal-Assisted Chemical Etching of Silicon: A Review, Adv. Mater., 23 (2011) 285-308.

[21] Y.-J. Hung, H.-W. Su, C.-L. Chun, J.-F. Chen, C.-W. Huang, M.-S. Cai, Enhanced Efficiency in Backside-Illuminated Deep-n-Well-Assisted CMOS Photovoltaic Devices, IEEE Electron Device Lett., 36 (2015) 1169-1171.

[22] C. Zhang, S.Z. Jiang, C. Yang, C.H. Li, Y.Y. Huo, X.Y. Liu, A.H. Liu, Q. Wei, S.S. Gao, X.G. Gao, B.Y. Man, Gold@Silver Bimetal Nanoparticles/Pyramidal Silicon 3D Substrate with High Reproducibility for High-Performance SERS, Sci. Rep., 6 (2016) 25243.

[23] H. Li, W. Hao, J. Hu, H. Wu, A photoelectrochemical sensor based on nickel hydroxyl-oxide

modified n-silicon electrode for hydrogen peroxide detection in an alkaline solution, Biosens. Bioelectron., 47 (2013) 225-230.

[24] S. Li, F. Zhang, L. Chen, H. Zhang, H. Li, Nickel oxyhydroxide-functionalized n-silicon photoelectrode for the photocurrent determination of Hg(II) ions at zero working voltage, Sens. Actuators, B, 257 (2018) 9-15.

[25] D.R. Gough, T.G. Cotter, Hydrogen peroxide: a Jekyll and Hyde signalling molecule, Cell Death Dis., 2 (2011) e213.

[26] W. Lei, A. Dürkop, Z. Lin, M. Wu, O.S. Wolfbeis, Detection of Hydrogen Peroxide in River Water via a Microplate Luminescence Assay with Time-Resolved ("Gated") Detection, Microchim. Acta, 143 (2003) 269-274.

[27] J.Z. Li, P.K. Dasgupta, Measurement of Atmospheric Hydrogen Peroxide and Hydroxymethyl Hydroperoxide with a Diffusion Scrubber and Light Emitting Diode-Liquid Core Waveguide-Based Fluorometry, Anal. Chem., 72 (2000) 5338-5347.

[28] R.A.D. Franchini, C.F. de Souza, R. Colombara, M.A.C. Matos, R.C. Matos, Rapid Determination of Hydrogen Peroxide Using Peroxidase Immobilized on Amberlite IRA-743 and Minerals in Honey, J. Agric. Food Chem., 55 (2007) 6885-6890.

[29] L. Campanella, R. Roversi, M.P. Sammartino, M. Tomassetti, Hydrogen peroxide determination in pharmaceutical formulations and cosmetics using a new catalase biosensor, J. Pharm. Biomed. Anal., 18 (1998) 105-116.

[30] N.V. Klassen, D. Marchington, H.C.E. McGowan, H_2O_2 Determination by the I_{3^-} Method and by $KMnO_4$ Titration, Anal. Chem., 66 (1994) 2921-2925.

[31] C. Matsubara, N. Kawamoto, K. Takamura, Oxo[5, 10, 15, 20-tetra(4-pyridyl)porphyrinato] Titanium(IV): An Ultra-High Sensitivity Spectrophotometric Reagent for Hydrogen Peroxide, Analyst, 117 (1992) 1781-1784.

[32] W. Lian, L. Wang, Y. Song, H. Yuan, S. Zhao, P. Li, L. Chen, A Hydrogen Peroxide Sensor Based on Electrochemically Roughened Silver Electrodes, Electrochim. Acta, 54 (2009) 4334-4339.

[33] A. Gutes, I. Laboriante, C. Carraro, R. Maboudian, Palladium Nanostructures from Galvanic Displacement as Hydrogen Peroxide Sensor, Sens. Actuators, B, 147 (2010) 681-686.

[34] S.J. Guo, D. Wen, Y.M. Zhai, S.J. Dong, E.K. Wang, Platinum Nanoparticle Ensemble-on-Graphene Hybrid Nanosheet: One-Pot, Rapid Synthesis, and Used as New Electrode Material for Electrochemical Sensing, ACS Nano, 4 (2010) 3959-3968.

[35] A.X. Gu, G.F. Wang, X.J. Zhang, B. Fang, Synthesis of CuO Nanoflower and Its Application as a H2O2 Sensor, Bull. Mat. Sci., 33 (2010) 17-20.

[36] W.J. Lan, C.C. Kuo, C.H. Chen, Hierarchical Nanostructures with Unique Y-Shaped Interconnection Networks in Manganese Substituted Cobalt Oxides: The Enhancement Effect on Electrochemical Sensing Performance, Chem. Commun., 49 (2013) 3025-3027.

[37] M. Li, Y. Xiong, X. Liu, X. Bo, Y. Zhang, C. Han, L. Guo, Facile Synthesis of Electrospun MFe_2O_4 (M = Co, Ni, Cu, Mn) Spinel Nanofibers with Excellent Electrocatalytic Properties for Oxygen Evolution and Hydrogen Peroxide Reduction, Nanoscale, 7 (2015) 8920-8930.

[38] J.J. Yin, X. Qi, L.W. Yang, G.L. Hao, J. Li, J.X. Zhong, A Hydrogen Peroxide Electrochemical Sensor Based on Silver Nanoparticles Decorated Silicon Nanowire Arrays, Electrochim. Acta, 56 (2011) 3884-3889.

[39] Q. Yan, Z. Wang, J. Zhang, H. Peng, X. Chen, H. Hou, C. Liu, Nickel Hydroxide Modified Silicon Nanowires Electrode for Hydrogen Peroxide Sensor Applications, Electrochim. Acta, 61 (2012) 148-153.

[40] Z.-c. Zhang, B. Xu, X. Wang, Engineering Nanointerfaces for Nanocatalysis, Chem. Soc. Rev., 43 (2014) 7870-7886.

[41] D. Brandon, W.D. Kaplan, Microstructural Characterization of Materials, 2nd Edition ed., John Wiley & Sons, Ltd., West Sussex, England, 2008.

[42] I. Zubel, I. Barycka, Silicon anisotropic etching in alkaline solutions I. The geometric description of figures developed under etching Si(100) in various solutions, Sens. Actuators, A, 70 (1998) 250-259.

[43] C.C. Kuo, W.J. Lan, C.H. Chen, Redox Preparation of Mixed-Valence Cobalt Manganese Oxide Nanostructured Materials: Highly Efficient Noble Metal-Free Electrocatalysts for Sensing Hydrogen Peroxide, Nanoscale, 6 (2014) 334-341.

[44] C.Y. Su, W.J. Lan, C.Y. Chu, X.J. Liu, W.Y. Kao, C.H. Chen, Photochemical Green Synthesis of Nanostructured Cobalt Oxides as Hydrogen Peroxide Redox for Bifunctional Sensing Application, Electrochim. Acta, 190 (2016) 588-595.

[45] T. Xiaorang, W. Qi, H. Hongtao, C. Guangyu, Z. Guanchao, Y. Rong, L. Liwei, M. Yuan, G. Ted, Pyramid size control and its effects on the performance of silicon heterojunction solar cells, 2015 China Semiconductor Technology International Conference, 2015, pp. 1-3.

[46] M. Ju, N. Balaji, C. Park, H.T. Thanh Nguyen, J. Cui, D. Oh, M. Jeon, J. Kang, G. Shim, J. Yi, The effect of small pyramid texturing on the enhanced passivation and efficiency of single c-Si solar cells, RSC Adv., 6 (2016) 49831-49838.

[47] J.T. Yates, Surface Chemistry of Silicon - The Behaviour of Dangling Bonds, J. Phys.-Condens. Matter, 3 (1991) S143-S156.

[48] K. Kitahara, K. Ohnishi, Y. Katoh, R. Yamazaki, T. Kurosawa, Analysis of Defects in

Polycrystalline Silicon Thin Films using Raman Scattering Spectroscopy, Jpn. J. Appl. Phys. Part 1 - Regul. Pap. Short Notes Rev. Pap., 42 (2003) 6742-6747.

[49] M. Schmitt, Analysis of Silanes and of Siloxanes Formation by Raman spectroscopy, RSC Adv., 4 (2014) 1907-1917.

[50] D.B. Lee, Anisotropic Etching of Silicon, J. Appl. Phys., 40 (1969) 4569-4574.

[51] P.J. Hesketh, C. Ju, S. Gowda, E. Zanoria, S. Danyluk, Surface Free Energy Model of Silicon Anisotropic Etching, J. Electrochem. Soc., 140 (1993) 1080-1085.

[52] M.K. Weilmeier, W.H. Rippard, R.A. Buhrman, Ballistic electron transport through Au(111)/Si(111) and Au(111)/Si(100) interfaces, Phys. Rev. B, 59 (1999) R2521-R2524.

[53] H. Choi, J. Gong, Y. Lim, K.H. Im, M. Jeon, Effects of the Electrical Conductivity and Orientation of Silicon Substrate on the Synthesis of Multi-Walled Carbon Nanotubes by Thermal Chemical Vapor Deposition, Nanoscale Res. Lett., 8 (2013) 110.

[54] R.T. Tung, The physics and chemistry of the Schottky barrier height, Appl. Phys. Rev., 1 (2014) 011304.

[55] R. Ludeke, A. Bauer, Hot electron scattering processes in metal films and at metal-semiconductor interfaces, Phys. Rev. Lett., 71 (1993) 1760-1763.

[56] S. Su, X.P. Wei, Y.Y. Guo, Y.L. Zhong, Y.Y. Su, Q. Huang, C.H. Fan, Y. He, A Silicon Nanowire-Based Electrochemical Sensor with High Sensitivity and Electrocatalytic Activity, Part. Part. Syst. Charact., 30 (2013) 326-331.

[57] B.R. Tao, R. Miao, H. Shao, F.J. Miao, Ag nanodendrites on silicon nanowire array for hydrogen peroxide sensing, Optoelectron. Adv. Mater.-Rapid Commun., 10 (2016) 945-949.

Graphical Abstract